168,

QPSK Carrier-Acquisition Performance in the Advanced Receiver II

S. Hinedi
Communications Systems Research Section

B. Shah
Radio Frequency and Microwave Subsystems Section

This article describes the frequency-acquisition performance of the Costas cross-over loop which is used in the Advanced Receiver II (ARX II) to perform Quadrature Phase Shift Keying (QPSK) carrier tracking. The performance of the Costas cross-over loop is compared to two other QPSK carrier tracking loops: the MAP estimation loop and the generalized Costas loop. Acquisition times and probabilities of acquisition as functions of both loop signal-to-noise ratio and frequency-offset to loop-bandwidth ratio are obtained using computer simulations for both type-II and type-III loops. It is shown that even though the MAP loop results in the smallest squaring loss for all signal-to-noise ratios, the MAP loop is sometimes outperformed by the other two loops in terms of acquisition time and probability.

I. Introduction

Quadrature Phase Shift Keying (QPSK) is an efficient modulation scheme which has been used extensively in communications systems. It offers a significant advantage over Binary Phase Shift Keying (BPSK) since it permits the transmission of twice the data rate in the same channel bandwidth [1], as both the in-phase and the quadrature components of the carrier are modulated. An even better use of bandwidth can be obtained by going to higher-order phase shift keying, but that would require a higher signal-to-noise ratio to achieve a required bit-error probability.

Depending on the application, derivatives of QPSK can also be used; these include Staggered QPSK (SQPSK), which is better suited for satellite channels with Travelling Wave Tube (TWT) amplifiers and Minimum Shift Keying (MSK), which can be thought of as SQPSK with sinusoidal pulse shapes.

One of the functional requirements of the Advanced Receiver II (ARX II) is that it acquire and track QPSK signals. The most likely candidate algorithm for the ARX II is the Costas cross-over loop because of its ease of implementation and relative performance. Carrier synchroniza-

tion for QPSK has been addressed by many authors in the literature and several loops have been introduced and analyzed in terms of their respective phase-error variance [2–4]. However, very little has been reported on the acquisition performance of these loops, mainly because the problem becomes highly nonlinear and precludes any analysis that provides insight into loop behavior. The suppressed carrier tracking loops are typically derived from Maximum A Posteriori (MAP) estimation theory; the derivative of the likelihood function is used as an error signal to provide a closed-loop implementation commonly referred to as *MAP estimation loops* [2].

Three QPSK loops are considered in this article in terms of their acquisition performance: the MAP estimation loop, the Costas cross-over loop (also known as the polarity-type Costas loop), and the generalized Costas loop (sometimes referred to as the conventional Costas loop). Mean acquisition times and probabilities of acquisition as functions of both loop signal-to-noise ratio (SNR) and frequency-offset-to-loop-bandwidth ratio are investigated using computer simulations for type-II and type-III loops.

The loops are all shown in Fig. 1 where different processing of the in-phase and quadrature channels identifies which loop is being implemented. The MAP estimation loop produces an error signal given by

$$Z_0 = Z_c \tanh(RZ_s) - Z_s \tanh(RZ_c) \qquad (1)$$

where R is the symbol SNR and Z_c, Z_s are the in-phase and quadrature signals respectively. This loop is "difficult" to build because it requires a priori knowledge of the symbol SNR and implementation of the hyperbolic tangent operations. The latter is hard to achieve in an analog fashion, but is easily done digitally with current technology using read-only memory (ROM) chips. To reduce the complexity of the MAP estimation loop, approximations to the hyperbolic tangent function can be used at low and high symbol SNRs. For instance, at high symbol SNRs, the hyperbolic tangent can be approximated by the signum function ($\tanh(x) \simeq \text{sgn}(x)$) to yield the Costas cross-over loop with error signal

$$Z_0 = Z_c \text{sgn}(Z_s) - Z_s \text{sgn}(Z_c) \qquad (2)$$

At low symbol SNRs, the nonlinearity hyperbolic tangent can be expanded using a Taylor series to give $\tanh(x) \simeq x - x^3/3$, which results in the generalized Costas loop with Z_0 given by

$$Z_0 = Z_c Z_s (Z_c^2 - Z_s^2) \qquad (3)$$

The two approximate loops are straightforward to implement and do not require knowledge of the symbol SNR. However, all three loops require an estimate of the incoming signal amplitude in order to operate the loop at the desired bandwidth.

Section II of this article develops a mathematical model for the various signals in Fig. 1. Simulation results are presented and discussed in Section III followed by the conclusion in Section IV.

II. Mathematical Model

In a typical communication system, the received signal is first downconverted to an appropriate intermediate frequency (IF) for further processing. At that point, the QPSK signal can be modeled as

$$r(t) = \sqrt{S}[d_I(t)\sin(\omega_i t + \theta) + d_Q(t)\cos(\omega_i t + \theta)] + n(t)$$

$$(4)$$

where S is the received power (watts), ω_i the IF radian frequency (rad/sec), θ the signal phase (rad), and $d_I(t)$, $d_Q(t)$ the in-phase and quadrature data streams given by

$$d_i(t) = \sum_{k=-\infty}^{+\infty} a_{k,i} p(t - kT) \quad i = I, Q \qquad (5)$$

where $p(t)$ is the baseband Non-Return-To-Zero (NRZ) pulse limited to T seconds and $a_{k,i}$ the equally likely ± 1 binary symbols. For SQPSK, the in-phase and quadrature baseband pulses will be offset by half a symbol period and for MSK, the pulses will be sinusoidal. The narrow-band noise process $n(t)$ can be expressed as

$$n(t) = \sqrt{2}n_c(t)\cos(\omega_i t + \theta) - \sqrt{2}n_s(t)\sin(\omega_i t + \theta) \qquad (6)$$

where $n_c(t)$ and $n_s(t)$ are statistically independent stationary band-limited white Gaussian noise processes with one-sided spectral density N_0 (watts/Hz) and one-sided bandwidth W (Hz). Assuming a digital implementation, the signal is first digitized at a high rate of R_s samples per sec ($T_s = 1/R_s$ is the sampling time) and subsequently demodulated using the in-phase and quadrature references (see Fig. 1). The resulting samples are then accumulated over a symbol duration and normalized to produce

$$Z_s(iT) = a_{i,I}\cos\phi - a_{i,Q}\sin\phi - N_I\cos\phi - N_Q\sin\phi \qquad (7)$$

$$Z_c(iT) = a_{i,I}\sin\phi + a_{i,Q}\cos\phi - N_I\sin\phi + N_Q\cos\phi \qquad (8)$$

where $\phi = \theta - \hat{\theta}$ is the phase error and N_I, N_Q are zero-mean Gaussian random variables with variances N_0/TS. It is assumed that perfect symbol synchronization has been achieved and no attempt is made to quantify the results of timing jitter on the carrier-acquisition process in this preliminary study. However, the acquisition performance with unknown symbol epoch is of prime interest as it reflects the carrier-acquisition process in a practical system. Moreover, the various loops might react differently in the absence of symbol synchronization and a complete study incorporating those effects is necessary. Depending on the loop, the error signal Z_0 is computed from Z_c and Z_s using the appropriate equations as discussed earlier. Further averaging over N symbols can be performed before updating the loop filter, which in turn controls the frequency of the numerically controlled oscillator (NCO).

The tracking performances of these loops have been derived elsewhere and are repeated below for convenience. In all cases, the variance of the phase-error process is given by

$$\sigma_\phi^2 = \frac{1}{\rho_c S_L} = \frac{1}{\rho} \tag{9}$$

where ρ is the loop SNR of the QPSK loop, $\rho_c = S/N_0 B_L$ the loop SNR of a "classical" phase-locked loop [1], and S_L is the "squaring" loss which for the MAP estimation loop is given by [2] as

$$S_L =$$

$$\frac{\overline{[\tanh(R - \sqrt{R}x) - R\,\text{sech}^2(R - \sqrt{R}x)]^2}}{\overline{(1 + R)\tanh^2(R - \sqrt{R}x)} - \overline{[(x - \sqrt{R})\tanh(R - \sqrt{R}x)]^2}} \tag{10}$$

where x is a zero-mean, unit-variance Gaussian random variable and the overbar denotes statistical expectation. For the Costas cross-over loop [3] $(\text{erf}(x) \triangleq (2/\sqrt{\pi}) \int_0^x e^{-t^2} dt$ denotes the error function), S_L becomes

$$S_L = \frac{[\text{erf}(\sqrt{R/2}) - \sqrt{2R/\pi}\,e^{-R/2}]^2}{1 + R - [\sqrt{2/\pi}\,e^{-R/2} + \sqrt{R}\,\text{erf}(\sqrt{R/2})]^2} \tag{11}$$

and

$$S_L = \frac{1}{1 + \frac{9}{2R} + \frac{6}{R^2} + \frac{3}{2R^3}} \tag{12}$$

for the conventional Costas loop [4]. In all cases, S_L is a function of only one parameter, the symbol SNR R defined as ST/N_0. Figure 2 depicts the "squaring" losses for the various loops; it is clear that the MAP estimation loop outperforms the other two loops for all values of R. For $R \geq 8$ dB, the performance of the Costas cross-over loop approaches that of the MAP loop. Similar arguments apply for the generalized loop at low SNRs ($R \leq -4$ dB). The analytical results were reproduced through computer simulations to obtain greater confidence in the programs before generating new results on acquisition.

III. Simulation Model, Results, and Discussion

The loops in Fig. 1 are simulated by generating the in-phase and quadrature signals Z_s and Z_c according to Eqs. (7) and (8). Depending on the loop under consideration, the instantaneous error signal Z_0 is computed using Eqs. (1), (2), or (3). The simulations were carried out assuming $N = 1$, i.e., the loop update rate is identical to the symbol rate. In this case, the NCO transfer function is given by

$$N(z) = \frac{T_u}{2} \frac{z+1}{z-1} \tag{13}$$

(where T_u denotes the loop update time) and it relates the filter output to the incoming phase estimate in the Z-domain. In some digital implementations, the NCO might have an additional delay, in which case the loop performance will be slightly worse than the one considered here. Unlike tracking, which depends solely on the loop bandwidth, acquisition behavior is a function of the loop filter itself and not just the loop bandwidth. The simulations were carried out with the following filter

$$F(z) = G_1 + \frac{G_2}{1 - z^{-1}} + \frac{G_3}{(1 - z^{-1})^2} \tag{14}$$

where

$$G_1 = rd/T_u \tag{15}$$

$$G_2 = rd^2/T_u \tag{16}$$

$$G_3 = krd^3/T_u \tag{17}$$

and

$$d = 4B_L T_u(r - k)/r(r - k + 1) \tag{18}$$

B_L denotes the design-loop bandwidth in Hz, r is typically 2 or 4 and is equal to 4ξ where ξ is the damping ratio, and k is a type-III loop gain parameter ($k = 0$ for a type-II loop) with typical values ranging from 1/4 to 1/2. The filter of Eq. (14) was derived from an equivalent analog filter using the Impulse Invariant Transformation (IIT) [5]. The actual loop bandwidth might be larger than the designed B_L depending on the product $B_L T_u$. Generally, for

$B_L T_u < 0.05$, the actual loop bandwidth is very close to the design loop bandwidth B_L.

Each simulation point was obtained using 5000 runs for each combination of loop SNR and frequency offset. Each run is for a maximum of $100/B_L$ seconds and the loop is declared to have acquired the incoming signal if the magnitude of the residual phase error becomes less than $\pi/8$ radians and remains there for at least $10/B_L$ seconds. By residual phase error is meant the phase error modulo $\pi/2$ since the stable lock points are integer multiples of $\pi/2$. The "acquisition" definition used in this article might be too strict for some applications, especially at low loop SNRs. This will be discussed later in more detail.

Since the acquisition results are based solely on computer simulations, it is worthwhile at this point to discuss their confidence level. Note that the outcome of each run is either "loop acquired" or "loop did not acquire," i.e., a binary decision. Let $\mathcal{X}$ be a random variable denoting the number of "loop acquired" decisions in n runs. Then, $\mathcal{X}$ can be modeled by a binomial distribution with mean np and variance $np(1 - p)$ where p denotes the expected probability of acquisition in a single run. Hence, the error level (ratio of the standard deviation to the mean) becomes $[(1 - p)/np]^{0.5}$ (accuracy level is $1 - [(1 - p)/np]^{0.5}$). As an example, when simulating the loops with an expected probability of acquisition of 10 percent using 5000 runs, the results will be correct with a 95.4-percent accuracy level. On the other hand, for a 90-percent probability of acquisition, the accuracy increases to 99.53 percent.

Probability of acquisition as a function of time (normalized by loop bandwidth) is depicted in Fig. 3 for all type-III loops and in Fig. 4 for all type II loops. It is clear that for a given acquisition time, the acquisition probability increases with decreasing frequency-offset-to-loop-bandwidth ratio $\Delta f/B_L$, as expected. Furthermore, type-II loops seem to outperform their respective type-III loops in terms of acquisition time for $\Delta f/B_L < 1$, but type-III loops are comparable for $\Delta f/B_L > 1$ for "high" acquisition probabilities. As an example, a type-II generalized Costas loop requires about $18/B_L$ seconds to acquire a $0.5B_L$-Hz frequency offset with a 60-percent probability, whereas the corresponding type-III loop requires about $30/B_L$ seconds for the same probability. On the other hand, when the frequency offset is about $1.25B_L$, then the type-II and type-III loops require about $90/B_L$ and $40/B_L$ seconds respectively for a 20-percent acquisition probability. This is better shown in Fig. 5 for the type-II and type-III Costas cross-over loops where either type can dominate depending on the ratio $\Delta f/B_L$. Note that at high probabilities of acquisition (> 90 percent), the

performance of type-II and type-III loops will become comparable as shown by the trends of Fig. 5 for $\Delta f/B_L = 0.75$ and 1.25, with type-II loops seemingly in the lead.

When comparing the different loop structures, the MAP estimation loop is sometimes outperformed by one or both of the other two loops; for example, at 50 percent acquisition probability with a frequency offset of $1.0B_L$ Hz, the MAP estimation loop and the Costas cross-over loop require about $73/B_L$ and $63/B_L$ seconds, respectively. This is an unexpected result but not very surprising as the MAP loop is the optimum closed-loop estimator for an unknown phase but not necessarily for an unknown frequency. Figures 6 and 7 compare the acquisition performance of the three different loops structures at 15- and 25-dB loop SNRs for both type-II and type-III loops. It seems that for type-II loops, the MAP loop is outperformed by both the Costas cross-over loop and the generalized Costas loop, depending on the loop SNR (Fig. 6); however, for type-III loops, the performance of the MAP loop is almost identical to the best of the other two loops (Fig. 7) for all practical purposes.

Another parameter of interest is the probability of acquisition assuming an unlimited acquisition time (simulations were actually carried out with $100/B_L$ seconds). This differs from the cumulative probability of acquisition plotted earlier which employs a fixed acquisition time. The probability of acquisition as a function of frequency-offset-to-loop-bandwidth ratio for a given loop SNR is plotted in Fig. 8 for type-II loops and in Fig. 9 for type-III loops. As expected, the probability increases with increasing loop SNR but decreases with increasing $\Delta f/B_L$. It is interesting to note that for both type-II and type-III loops, the MAP estimation loop for all practical purposes achieves the highest probability of acquisition for a given loop SNR and a fixed $\Delta f/B_L$. However, from the previous discussion, the MAP loop does not necessarily have the highest probability of acquisition for a fixed acquisition time.

Finally, Fig. 10 depicts the effect of $B_L T_u$ on the cumulative probability for the Costas cross-over loop. As expected, better performance is obtained by decreasing $B_L T_u$, which results in a faster loop update rate for a given loop bandwidth.

As mentioned earlier, the acquisition definition invoked so far might be too strict at low loop SNRs. This is because even though the loop can acquire the incoming phase (i.e., the residual phase error becomes less than $\pi/8$ as required), it cannot remain there for $10/B_L$ seconds because the mean time to lose lock at low loop SNR becomes "small" and affects the probability of acquisition. This is

illustrated in Fig. 11, where the cumulative probability of acquisition is plotted against $B_L t$ for different lock criteria for the Costas cross-over loop at both 15- and 20-dB loop SNRs. For a 20-dB loop SNR, the cumulative probability of acquisition is for all practical purposes independent of the lock criterion used because the mean time to lose lock is larger than the $10/B_L$ seconds required. However, for a 15-dB loop SNR, the mean time to lose lock is small compared to $10/B_L$ seconds and the performance varies with each lock criterion as expected. In that sense, the lock criterion of $10/B_L$ seconds might not be fair for low loop SNRs.

IV. Conclusion

Three QPSK carrier tracking loops were compared in this article in terms of their acquisition performance. It was determined that the Costas cross-over loop is the most likely candidate for implementation in the ARX II due to its simplicity and overall relative performance.

References

[1] W. C. Lindsey and M. K. Simon, *Telecommunication Systems Engineering*, Inglewood Cliffs, New Jersey: Prentice-Hall Inc., 1973.

[2] M. K. Simon, "On the Optimality of the MAP Estimation Loop for Carrier Phase Tracking BPSK and QPSK Signals," *IEEE Trans. on Communications*, vol. COM-27, no. 1, pp. 158–165, January 1979.

[3] W. R. Braun and W. C. Lindsey, "Carrier Synchronization Techniques for Unbalanced QPSK Signals—Part I," *IEEE Trans on Communications*, vol. COM-26, no. 9, pp. 1325–1333, September 1978.

[4] J. J. Stiffler, *Theory of Synchronous Communications*, Inglewood Cliffs, New Jersey: Prentice-Hall Inc., 1971.

[5] S. Aguirre, W. Hurd, R. Kumar, and J. Statman, "A Comparison of Methods for DPLL Loop Filter Design," *TDA Progress Report 42-87*, vol. July-September 1986, Jet Propulsion Laboratory, Pasadena, California, pp. 114–124, November 15, 1986.
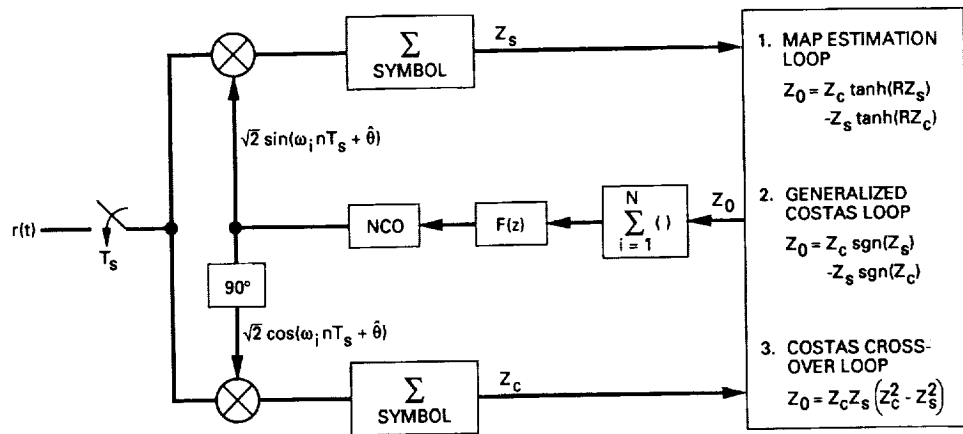
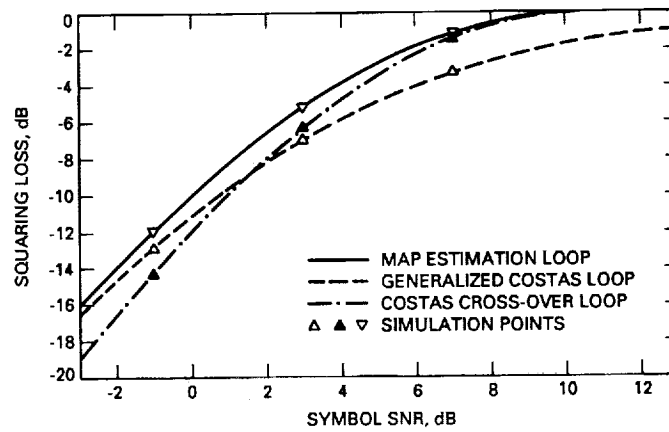Fig. 1. The QPSK carrier-tracking loops.
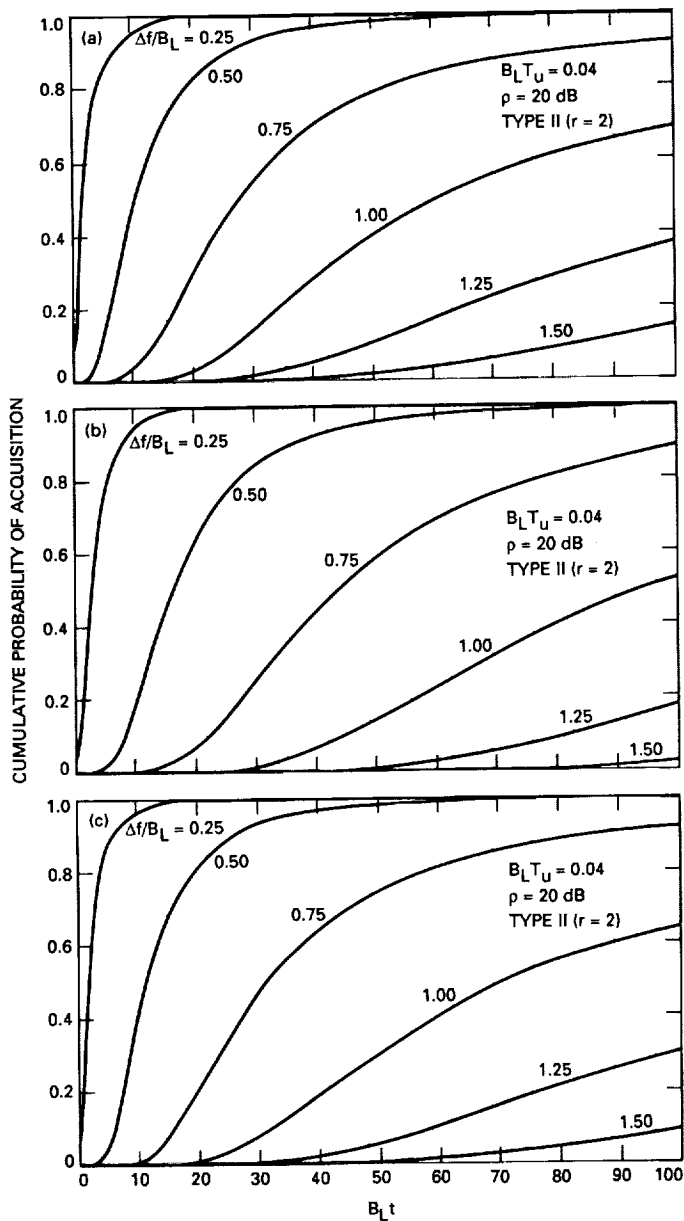

Fig. 2. Squaring losses of the QPSK loops.

Fig. 3. Cumulative probability of acquisition versus $B_L t$ for type-II loops: (a) Costas cross-over loop, (b) generalized Costas loop, and (c) MAP estimation loop.
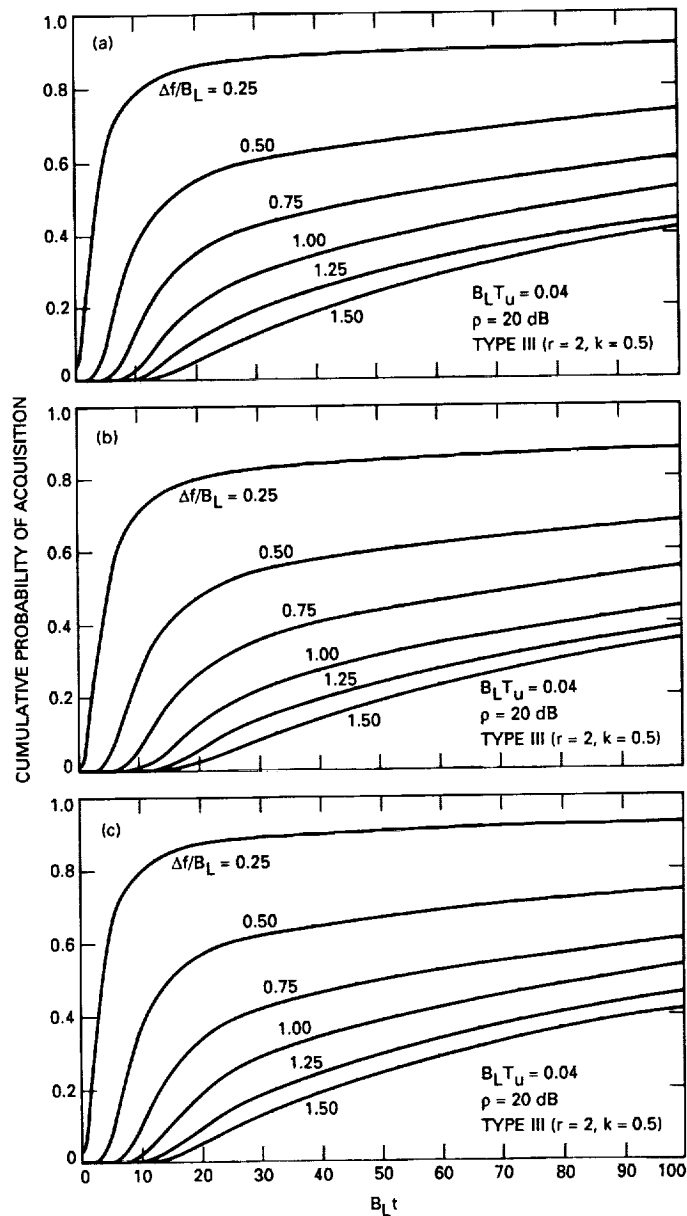
Fig. 4. Cumulative probability of acquisition versus $B_L t$ for type-III loops: (a) Costas cross-over loop, (b) generalized Costas loop, and (c) MAP estimation loop.
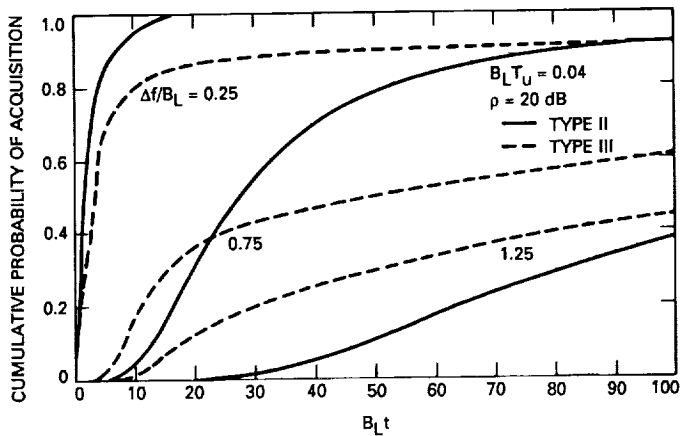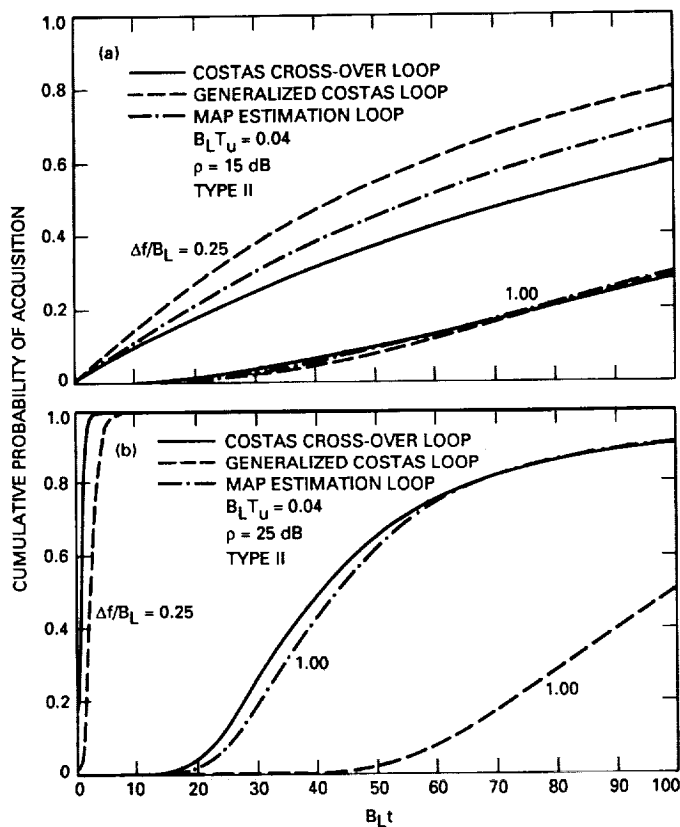
156

Fig. 5. Cumulative probability of acquisition versus $B_L t$ for the type-II and -III Costas cross-over loops.

Fig. 6. Cumulative probability of acquisition versus $B_L t$ for all three type-II loops: (a) $\rho = 15$ dB and (b) $\rho = 25$ dB.
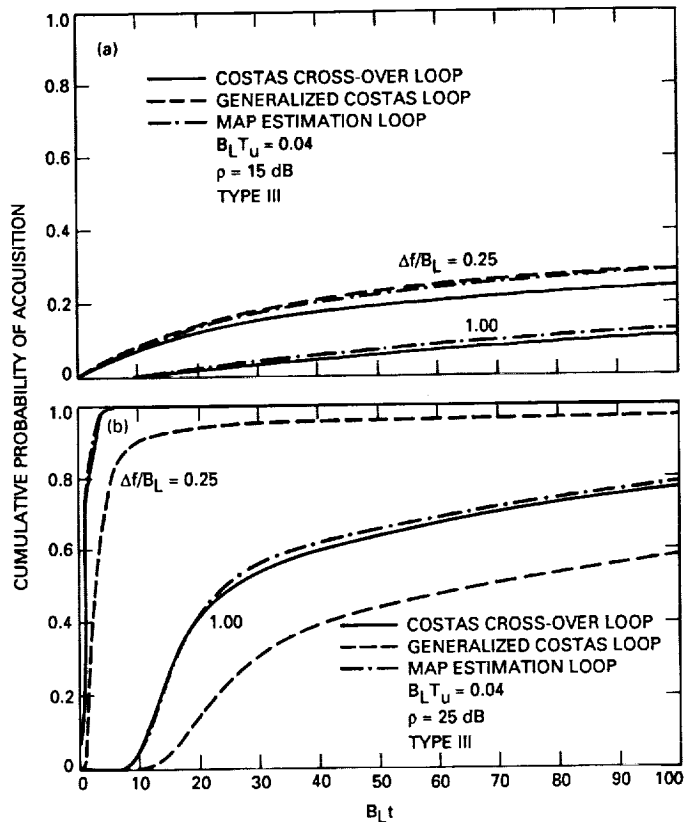
Fig. 7. Cumulative probability of acquisition versus $B_L t$ for all three type-III loops: (a) $\rho = 15$ dB and (b) $\rho = 25$ dB.
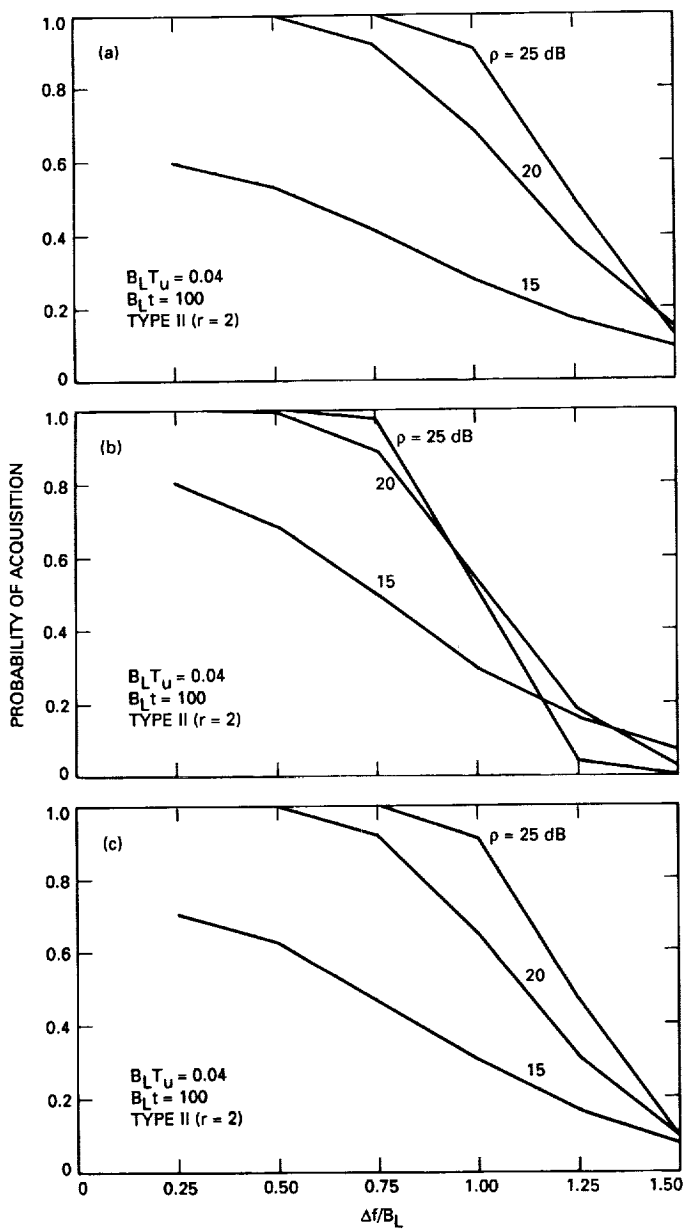
157

Fig. 8. Probability of acquisition versus $\Delta f/B_L$ for type-II loops: (a) Costas cross-over loop, (b) generalized Costas loop, and (c) MAP estimation loop.
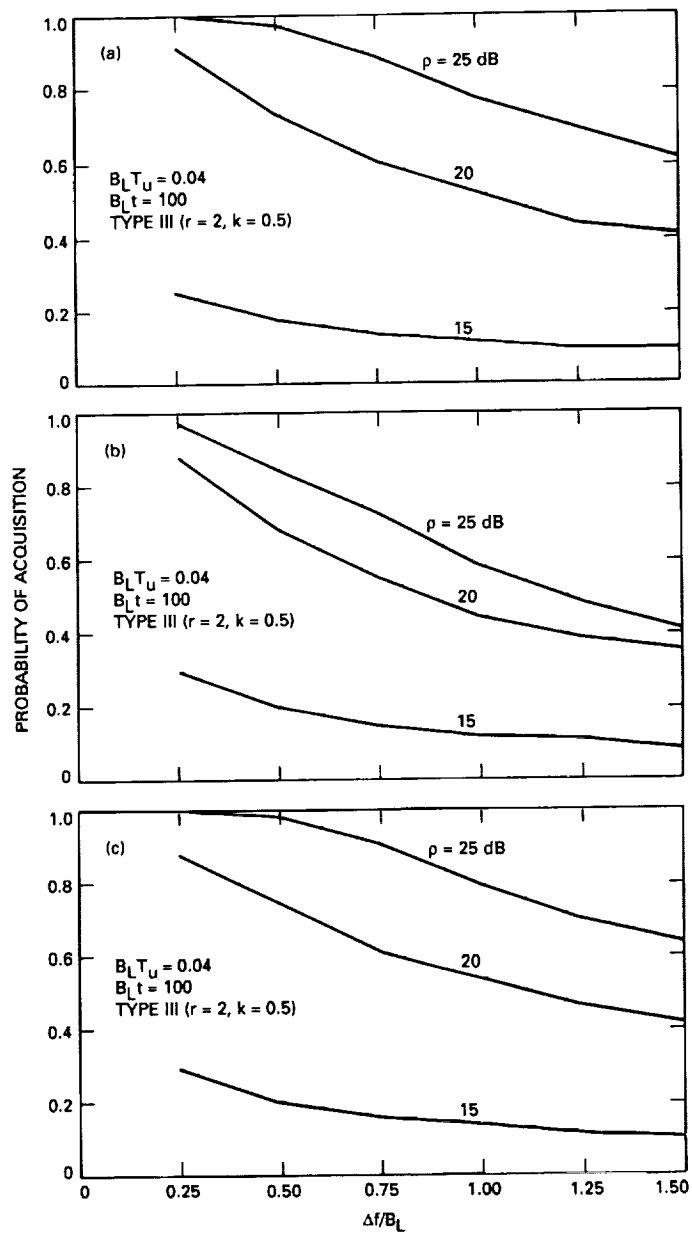
Fig. 9. Probability of acquisition versus $\Delta f/B_L$ for type-III loops: (a) Costas cross-over loop, (b) generalized Costas loop, and (c) MAP estimation loop.
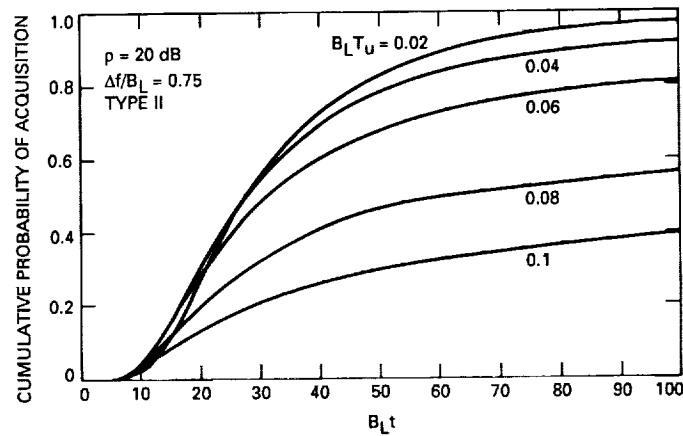
Fig. 10. Cumulative probability of acquisition versus $B_L t$ for the Costas cross-over loop for varying $B_L T_u$.
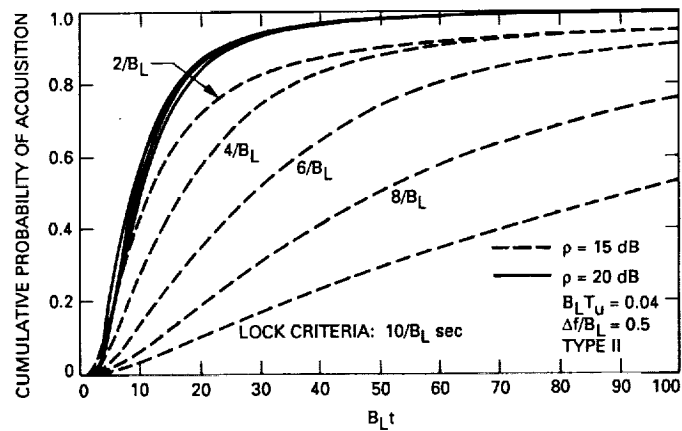

Fig. 11. Cumulative probability of acquisition versus $B_L t$ for the Costas cross-over loop for different lock criteria.